Available online at www.sciencedirect.com
ScienceDirect
Ceramics International 35 (2009) 2693–2698
CERAMICS INTERNATIONAL
www.elsevier.com/locate/ceramint

Optical properties of TiO_2 nanoceramic films as a function of N–Al co-doping

Su-Shia Lin *

Department of Applied Materials and Optoelectronic Engineering, National Chi Nan University, Puli, Nantou Hsien 54561, Taiwan, ROC

Received 9 December 2008; received in revised form 12 January 2009; accepted 2 March 2009
Available online 1 April 2009

Abstract

The N-doped TiO_2, Al-doped TiO_2 and N–Al co-doped TiO_2 films had the similar structure to that of the TiO_2 film and corresponded to nanocrystalline anatase. By N and/or Al doping, the TiO_2 film became more stoichiometric and the nanocrystallinity was enhanced, especially N–Al co-doping. The optical transmission of N–Al co-doped TiO_2 film was the highest because of the lowest surface roughness and the lowest porosity. The nonlinear refractive index of N–Al co-doped TiO_2 film on the glass substrate was measured by Moiré deflectometry, and was of the order of 10^{-8} cm^2 W^{-1}. By N–Al co-doping, the TiO_2 nanoceramic film exhibited highest linear refractive index, lowest stress and lowest stress-optical coefficient.

Keywords: Porosity; N–Al co-doped TiO_2 film; Transmission; Refractive index

1. Introduction

Among the numerous oxide materials, titanium dioxide (TiO_2) has received unprecedented interest due to its superior physical, chemical properties, high stability and ability to be easily doped with active ions. It was considered for various optical applications such as high refractive index component of multilayer optical filter, gas sensors, antireflective coating, photocatalysts, and planar waveguides [1–3]. TiO_2 thin films have been prepared by several techniques, including spray pyrolysis [4], sol–gel method [5], chemical vapor deposition [6], ion-assisted electron beam evaporation [7], atomic layer deposition [8], sputtering [9] and pulsed laser deposition (PLD) [10].

Titanium dioxide has three phases in nature—anatase, rutile and brookite. Structural changes may occur during the heating process [11]. Such structural changes lead to complications for optical characterization and the quality control of TiO_2 films [12–16]. Several dopants, such as Ce and W [17], Cu [18], Nb and Cr [19], Pt [20], etc., have been used to dope TiO_2. However, few studies of N–Al co-doped TiO_2 films have been reported. Without heating the substrates, the effects of N and/or Al dopants on the optical properties of TiO_2 films were investigated in this study.

Transparent materials generally exhibit the optical Kerr effect. The nonlinear refractive indices of materials are of great interest because of their potential applications in designing optical devices and laser technology [21–24]. Moiré deflectometry is a powerful tool for measuring the nonlinear refractive indices of materials. The main advantages of the Moiré deflectometry technique are its extreme experimental simplicity, lower cost and lower sensitivity to external disturbances than other interferometric methods. In this study, this method is applied to measure the nonlinear refractive indices of N–Al co-doped TiO_2 films on glass substrates under illumination with a 5-mW He–Ne laser (λ = 632.8 nm).

2. Experimental procedures

The N–Al co-doped TiO_2 films were deposited on glass (Corning 1737) by simultaneous rf magnetron sputtering of TiO_2 and dc magnetron sputtering of Al. The dimension of the glass substrates was 24 mm × 24 mm × 1.1 mm. Before deposition, the substrates were ultrasonically cleaned in alcohol, rinsed in deionized water and dried in nitrogen. Two circular targets were used (5 cm diameter, 5 mm thickness); the first was sintered

* Tel.: +886 49 2910960x4771; fax: +886 49 2912238.
E-mail address: sushia@ncnu.edu.tw.

0272-8842/$36.00
doi:10.1016/j.ceramint.2009.03.015

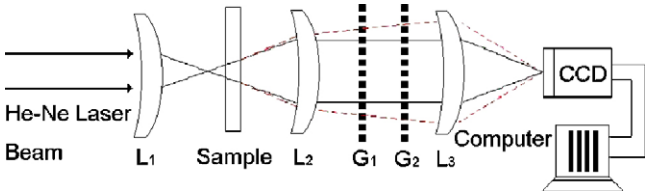

Fig. 1. The experimental set-up for measuring index of nonlinear refraction by Moiré deflectometry technique.

stoichiometric TiO_2 (99.99% purity); the other was metallic Al (99.999% purity).

The sputtering was performed in a mixed Ar–N_2 atmosphere with a target-to-substrate distance of 15 cm. A turbo-molecular pump, backed by a rotary pump, was used to achieve a base pressure of 1.3×10^{-4} Pa. For the deposition of the films, the substrates were not heated. The chamber was back-filled with a mixed Ar–N_2 atmosphere at a working pressure of 1.5 Pa. The gas flow rates of argon and nitrogen were 43 and 10 sccm, respectively. An rf power (13.56 MHz, RGN CONTROLLER, ULVAC, Japan) of 50 W was supplied to the TiO_2 target, and a dc power (DCS0052B, ULVAC, Japan) of 4 W was applied to the Al target. No external bias voltage was applied to substrate. The rotating speed of the substrate was 20 rpm, and the thickness of films was in the range of 20–120 nm.

The film thickness was measured using a surface profiler (Alpha-Step 500, TENCOR, Santa Clara, CA). X-ray diffraction (XRD; Rigaku D/MAX2500, Japan) was used to study the crystal structure. The elemental compositions were investigated by X-ray photoemission spectroscopy (XPS; PHI 5000 VersaProbe, Japan). The surface morphologies and surface roughness were examined by atomic force microscopy (AFM; Agilent 5500, Santa Clara, CA). The linear refractive indices of films were recorded using a spectrometer (MP100-ST, Fremont, CA). The stress was measured by Nano Indenter XP System (MTS Systems Corporation, MN USA). The optical transmission spectra of films in the visible-infrared (VIS-IR) region were obtained using a spectrophotometer (HP 8452A diode array spectrophotometer, Hewlett Packard, Palo Alto, CA).

Fig. 1 shows the Moiré deflectometry experimental set-up that is used to measure the nonlinear refractive indices of N–Al co-doped TiO_2 films on glass substrates. Lens L_1 focused a 5-mW He–Ne laser beam (wavelength of 632.8 nm), which was re-collimated by lens L_2. The focal lengths of lenses L_1, L_2 and L_3 were all −250 mm. Two similar Ronchi gratings G_1 and G_2 with a pitch of 0.1 mm were used to construct the Moiré fringe patterns. The distance between the planes of G_1 and G_2 was set to 64 mm, which is one of the Talbot distances of the used gratings. The Talbot distances satisfy $z_t = tp^2/\lambda$ where p is the periodicity of the grating; λ is the wavelength of light, and t is an integer. In this work, the Moiré fringes were clearly formed for a Talbot distance of $z_{t=4} \approx 4$ mm, indicating that the Moiré fringes were observed on a screen attached to the second grating. The Moiré fringe patterns were projected onto a computerized CCD camera by lens L_3, which was placed at the back of the second grating.

3. Results and discussion

3.1. Structural characterization

Table 1 shows the results of elemental composition analysis of the different doped TiO_2 films detected by XPS. The N–Al co-doped TiO_2 film had higher O/(Ti + N + Al) atomic ratio, suggesting that the TiO_2 films became more stoichiometric by N–Al co-doping.

Fig. 2 shows the X-ray diffraction patterns of different doped TiO_2 films. XRD analysis was conducted on the films using a Rigaku D/MAX2500 goniometer with 18 kW rotating anode X-ray, equipped with a thin film attachment unit. The equipment was operated with Cu Kα (λ = 1.5418 Å) radiation at 40 kV, 100 mA and a scanning speed of 4° min^{-1} at an incident angle of 3°. The interval of the scan was 0.01° and the scanning range was $10–70^\circ$. From Fig. 2, it can be found that there is a broad diffraction peak (1 0 1) corresponding to nanocrystalline anatase TiO_2 film. Nanocrystalline rutile and anatase could be obtained also with low temperature synthesis; the crystallization and

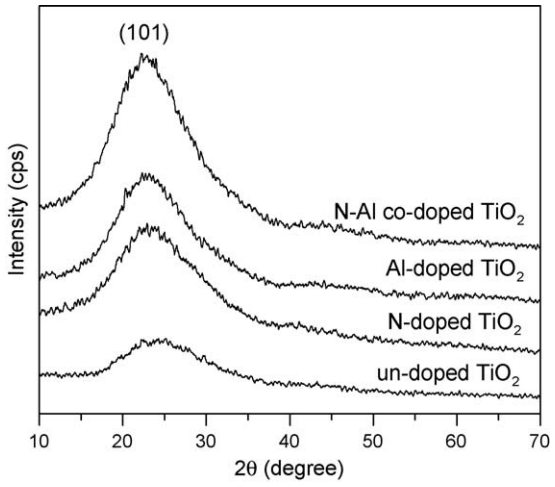

Fig. 2. The X-ray diffraction patterns of different doped TiO_2 films.

Table 1
Elemental composition of the different doped TiO_2 films was obtained by XPS.

Film	O content (at.%)	Ti content (at.%)	N content (at.%)	Al content (at.%)	O/(Ti + N + Al)
Un-doped TiO_2	60.1	39.9	0	0	1.51
N-doped TiO_2	62.9	35.3	1.8	0	1.70
Al-doped TiO_2	62.7	35.6	0	1.7	1.68
N–Al co-doped TiO_2	63.5	32.9	1.9	1.7	1.73

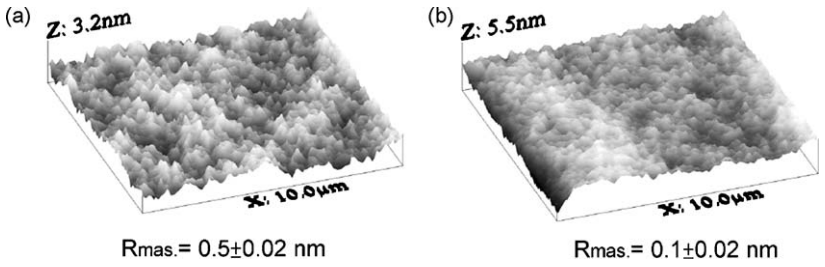

Fig. 3. The morphologies of (a) un-doped TiO_2 and (b) N–Al co-doped TiO_2 film.

transformation temperatures have a great variability and strongly depend from a large number of parameters [25].

Compared with TiO_2, N-doped TiO_2 film, Al-doped TiO_2 film and N–Al co-doped TiO_2 film showed the stronger peak (1 0 1) and the location of the measured diffraction peak shifted towards the lower diffraction angle as N and/or Al atoms were doped. It indicated that the nanocrystallite of TiO_2 film was changed by N and/or Al atoms substituting in the Ti sites [26]. The crystal sizes of all the deposited films were calculated using Scherrer's formula [27,28]:

$$D = \frac{0.9\lambda}{\beta \cos\theta} \tag{1}$$

where $\lambda = 1.5418$ Å and $\beta = B - b$, where B is the observed FWHM and b is the instrument function determined from the broadening of the monocrystalline silicon diffraction line. The crystal sizes of all the deposited films were similar, and estimated to be 8–10 nm.

Bachari et al. [29] reported that the oxygen deficiency leaded to the growth of less homogeneous films with more crystallographic faults, and a decrease in the long-range order in the deposited films. It suggested that the non-stoichiometric films displayed poor crystallinity. Similarly, TiO_2 films showed stronger peaks (1 0 1) due to more stoichiometric when N and/or Al atoms were doped. It indicated that the nanocrystallinity was enhanced as N and/or Al atoms were doped.

Fig. 3 shows the morphologies of (a) un-doped TiO_2 and (b) N–Al co-doped TiO_2 film. The N–Al co-doped TiO_2 film nucleated as continuous islands and showed the lowest surface roughness. The roughness values were very close to the morphologies of growing films [30].

3.2. Optical characterization

The index of refraction, n, which depends on the radiation intensity, may be expressed in terms of the nonlinear index n_2 ($cm^2\ W^{-1}$):

$$n(r,z) = n_0 + n_2 I(r,z) = n_0 + \Delta n(r,z) \tag{2}$$

where n_0 is the linear index of refraction, $I(r, z)$ is the irradiance of the laser beam within the sample, and $\Delta n(r, z)$ is the light-induced change in refractive index. Based on the assumption that a Gaussian beam is traveling in the $+z$ direction, the beam irradiance can be written as

$$I(r,z) = I_0 \frac{\omega_0^2}{\omega^2(z)} \exp\left[-\frac{2r^2}{\omega^2(z)}\right] \tag{3}$$

where r is the radial radius of the imaginary sphere; ω_0 is the spot size of the beam at the focus; $\omega(z) = \omega_0(1 + z^2/z_0^2)^{1/2}$ is the beam radius at a distance z from the position of the waist; $z_0 = \pi\omega_0^2/\lambda$ is the diffraction length of the Gaussian beam, and λ is the wavelength. The irradiance of the beam at the focus is denoted I_0 and in terms of the input laser power, p_{in}, equals $2p_{in}/\pi\omega_0^2$. Therefore, for a Gaussian laser beam, the radial dependence of the irradiance gives rise to a radially dependent parabolic refractive index change near the beam axis:

$$\Delta n(r,z) = n_2 I_0 \frac{\omega_0^2}{\omega^2(z)} \exp\left[-\frac{2r^2}{\omega^2(z)}\right] \tag{4}$$

Moiré deflectometry is a sensitive technique for measuring changes in the refractive indices of materials. The sensitivity of this technique is determined by the minimum measurable angle of rotation (α_{min}). Fig. 4 shows the Moiré fringe rotation angle versus z for the N–Al co-doped TiO_2 film on glass substrate. The tested sample was placed at various distances from the focal point of lens L_1. The minimum angle of rotation was obtained from the figure. The same experiment was performed using only a pure glass substrate to check the contribution of the glass substrate to the nonlinear refraction measurement. No observed fringe rotation or change in fringe size was found.

For the thin nonlinear medium of thickness d, the lowest nonlinear refractive index can be written as

$$n_{2,\min} = \frac{\theta f_2^2}{z_t} \frac{\pi\omega_0^4}{d p_{in} z_0^2} \alpha_{\min} \tag{5}$$

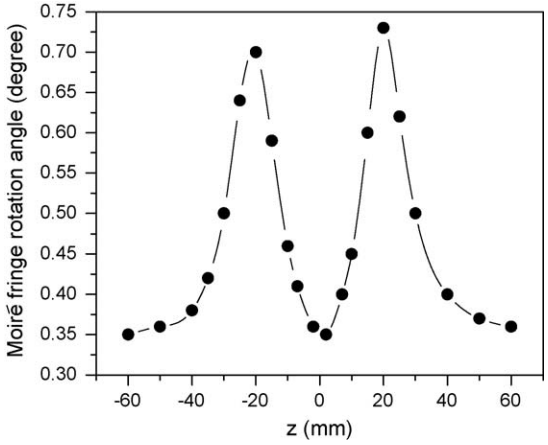

Fig. 4. The Moiré fringe rotation angle vs. z for the N–Al co-doped TiO_2 film on glass substrate.

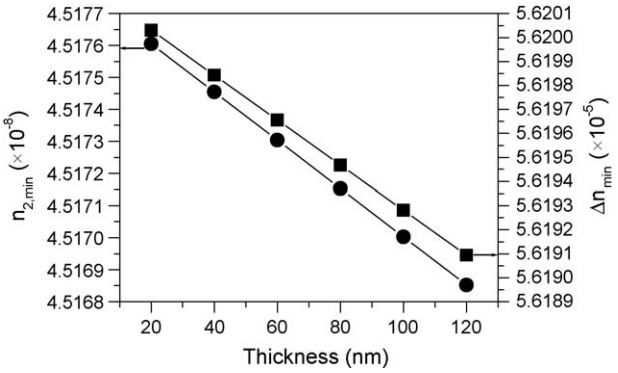

Fig. 5. The minimum nonlinear refractive index and the change in the minimum refractive index of N–Al co-doped TiO_2 film prepared at different thickness on glass substrate.

and the change in the minimum refractive index is

$$\Delta n_{\min} = \frac{\omega_0^2 \theta f_2^2}{2 d z_t z_0^2} \alpha_{\min} \tag{6}$$

Fig. 5 shows the minimum nonlinear refractive index and the change in the minimum refractive index of N–Al co-doped TiO_2 film prepared at different thickness on glass substrate. The nonlinear refraction index was measured to be of the order of 10^{-8} cm^2 W^{-1} and the change in refractive index was of the order of 10^{-5}.

Fig. 6 shows the Moiré fringe patterns of different doped TiO_2 films on glass substrates. By comparing Fig. 6a with b, the changes in sizes of the Moiré fringes were observed. It was probably due to the more pores in un-doped TiO_2 films. According to Fig. 6b–d, there were no rotation or changes in sizes of the Moiré fringes. It suggested that the amounts of pores were not obvious difference as TiO_2 films were doped with N and/or Al.

Table 2
Linear refractive index, porosity and Young's modulus of the different doped TiO_2 films.

Film	Linear refractive index, n_0	Porosity (%)	Young's modulus (GPa)
Un-doped TiO_2	2.036 ± 0.0005	41.1 ± 0.08	72 ± 0.3
N-doped TiO_2	2.278 ± 0.0006	21.6 ± 0.05	60 ± 0.3
Al-doped TiO_2	2.275 ± 0.0008	21.8 ± 0.09	62 ± 0.7
N–Al co-doped TiO_2	2.289 ± 0.0004	20.7 ± 0.03	58 ± 0.2

Table 2 shows linear refractive index, porosity and Young's modulus of the different doped TiO_2 films. The linear refractive index n_0 was measured at a wavelength of 632.8 nm. The N–Al co-doped TiO_2 film had the highest linear refractive index. The linear refractive index was found to correlate with the porosity [31]. In this study, all the deposited films are assumed to be homogeneous. The porosity of the thin films can be calculated using the following equation [32]:

$$\text{porosity}\,(\%) = \left(1 - \frac{n_0^2 - 1}{n_a^2 - 1}\right) \times 100 \tag{7}$$

where n_0 is the linear refractive index of the porous thin film and n_a is the linear refractive index of pore-free anatase

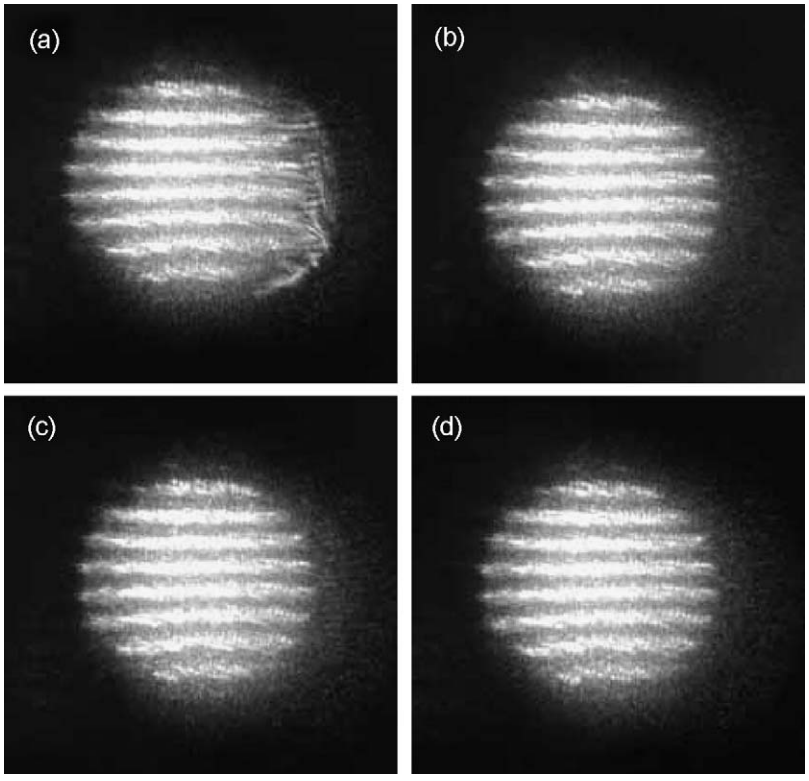

Fig. 6. The Moiré fringe patterns of (a) un-doped TiO_2, (b) N-doped TiO_2, (c) Al-doped TiO_2, and (d) N–Al co-doped TiO_2 films on glass substrates.

(n_a = 2.52) found in the literature [33]. The porosity of the N–Al co-doped TiO_2 film was the lowest.

A change of the linear refractive index caused by stress is called the photoelastic effect [34]. The linear refractive index is specified by the indicatrix, which is an ellipsoid whose coefficients are the components of the relative dielectric impermeability tensor B_{ij} at optical frequencies:

$$B_{ij}x_i x_j = 1 \tag{8}$$

The small change of the linear refractive index produced by stress is a small change in the shape, size and orientation of the indicatrix. This change is specified by the small changes in the coefficients B_{ij}.

If terms of higher order than the first in the field of stresses are neglected, then the changes ΔB_{ij} in the coefficients are

$$\Delta B_{ij} = \varphi_{ijkl}\sigma_{kl} \quad \text{or} \quad \Delta B_{ij} = p_{ijrs}\varepsilon_{rs} \tag{9}$$

where φ_{ijkl} and p_{ijrs} are called the piezo-optical and strain-optical coefficients, which typically have the orders of magnitude of 10^{-12} and 10^{-1} Pa^{-1}, respectively.

Based on the relation, $B = 1/n_0^2$, the change of linear refractive index for an isotropic film material is assumed to be [34,35]:

$$\left(\frac{\partial n_0}{\partial \sigma}\right)_T = -\frac{1}{2}n_0^3\varphi \tag{10}$$

Consequently, a change in the linear refractive index due to film stress may affect the optical performance of an optical thin film, as shown in Eq. (10).

From Table 2, the linear refractive index of N–Al co-doped TiO_2 film was the highest. However, the stress of N–Al co-doped TiO_2 film was the lowest. The value of $\Delta n/\Delta\sigma$ is reportedly similar to the stress-optical coefficient [36]. The stress-optical coefficient, $(\partial n_0/\partial\sigma)_T$, of a N–Al co-doped TiO_2 film was the lowest, and evaluated to be in the range of -17.9×10^{-12} to -20.1×10^{-12} Pa^{-1}.

Fig. 7 shows the transmission in the VIS-IR region of different doped TiO_2 films. The optical transmission of N–Al co-doped TiO_2 film was the highest, especially in the visible region. It was probably due to the relatively low surface roughness, which could result in less light scattering [37]. It was also probably due to the lowest porosity, which absorbing less light [38]. Similar results were reported by Yu et al. [38] and Lin and Huang. [39].

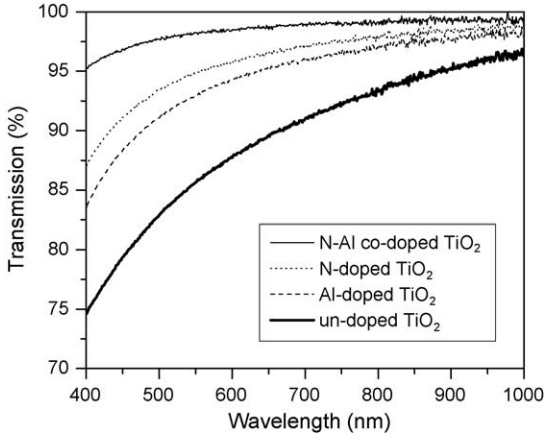

Fig. 7. The transmission in the VIS-IR region of different doped TiO_2 films.

4. Conclusions

The N-doped TiO_2, Al-doped TiO_2 and N–Al co-doped TiO_2 films had the similar structure to that of the TiO_2 film and corresponded to nanocrystalline anatase. By N–Al co-doping, the TiO_2 film became more stoichiometric and the nanocrystallinity was enhanced. The N–Al co-doped TiO_2 film had lowest surface roughness and lowest porosity, which resulted in the highest optical transmission, especially in the visible region. The nonlinear refraction index of the N–Al co-doped TiO_2 film on the glass substrate was measured to be of the order of 10^{-8} cm^2 W^{-1} and the change in the refractive index was of the order of 10^{-5}. Furthermore, the N–Al co-doped TiO_2 film had highest linear refractive index, lowest stress and lowest stress-optical coefficient.

Acknowledgement

The author would like to thank the National Science Council of the Republic of China, Taiwan, for financially supporting this research under Contract No. NSC-97-2221-E-260-004.

References

[1] D.P. Partlow, T.W. O'Keeffe, Appl. Opt. 29 (10) (1990) 1526.
[2] A. Brunik, H. Cztemastek, K. Zakrzewska, M. Jachimowski, Thin Solid Films 199 (1) (1991) 45.
[3] L. Yang, S. Scott Saavedra, N.R. Armstrong, J. Hayes, Anal. Chem. 66 (8) (1994) 1254.
[4] D. Li, H. Haneda, S. Hishita, N. Ohashi, Mater. Sci. Eng. B 117 (2005) 67.
[5] N. Venkatachalam, A. Vinu, S. Anandan, B. Arabindoo, V. Murugesan, J. Nanosci. Nanotechnol. 6 (2006) 2499.
[6] Y. Guo, X.W. Zhang, G.R. Han, Mater. Sci. Eng. B 135 (2006) 83.
[7] T.S. Yang, M.C. Yang, C.B. Shiu, W.K. Chang, M.S. Wong, Appl. Surf. Sci. 252 (2006) 3729.
[8] V. Pore, M. Heikkila, M. Ritala, M. Leskela, S. Areva, J. Photochem. Photobiol. A 177 (2006) 68.
[9] S.H. Mohamed, O. Kappertz, T. Niemeier, R. Drese, M.M. Wakkad, M. Wutting, Thin Solid Films 468 (2004) 48.
[10] P. Xu, L. Mi, P.N. Wang, J. Cryst. Growth 289 (2006) 433.
[11] L. Sun, P. Hou, Thin Solid Films 455–456 (2004) 525.
[12] H.K. Jang, Y.S. Lee, T.K. Kim, J. Vac. Sci. Technol. A 18 (2000) 2932.
[13] J.D. Deloach, C.R. Aita, J. Vac. Sci. Technol. A 16 (1998) 1963.
[14] J.V. Grahn, M. Linder, E. Fredriksson, J. Vac. Sci. Technol. A 16 (1998) 2495.
[15] Y. Yasumi, U. Haruo, W. Shigeyuki, N. Hisakazu, Appl. Opt. 38 (1999) 6638.
[16] D. Mardare, A. Stancu, Mater. Res. Bull. 35 (2000) 2017.
[17] L. Zheng, Sens. Actuators B 94 (2003) 294.
[18] N.O. Savage, S.A. Akbar, P.K. Dutta, Sens. Actuators B 72 (2001) 239.
[19] K. Zakrzewska, Vacuum 74 (2004) 335.
[20] J. Trimboli, P.K. Dutta, Sens. Actuators B 102 (2004) 132.
[21] M.J. Soileau, W.E. Williams, N. Mansour, E.W. Van Stryland, Opt. Eng. 28 (1989) 1133.
[22] E.W. Van Stryland, Y.Y. Wu, D.J. Hagan, M.J. Soileau, K. Mansour, J. Opt. Soc. Am. B 5 (1988) 1980.

[23] M.J. Soileau, W.E. Williams, E.W. Van Stryland, IEEE J. Q. Elect. QE-19 (1983) 731.
[24] K. Mansour, M.J. Soileau, E.W. Van Stryland, J. Opt. Soc. Am. B 3 (1992) 1100.
[25] Y. Djaoued, S. Badilescu, P.V. Ashrit, D. Bersani, P.P. Lottici, R. Bruening, J. Sol-Gel Sci. Technol. 24 (2002) 247.
[26] S.S. Lin, J.L. Huang, P. Šajgalik, Surf. Coat. Technol. 191 (2–3) (2005) 286.
[27] L. Sagalowicz, G.R. Fox, J. Mater. Res. 14 (1999) 1876.
[28] G. Sanon, R. Rup, A. Mansingh, Thin Solid Films 190 (1990) 287.
[29] E.M. Bachari, G. Baud, S. Ben Amor, M. Jacquet, Thin Solid Films 348 (1999) 165.
[30] G. Laukaitis, S. Lindroos, S. Tamulevičius, M. Leskelä, Appl. Surf. Sci. 185 (2001) 134.
[31] G.S. Vicente, A. Morales, M.T. Gutierrez, Thin Solid Films 391 (2001) 133.
[32] B.E. Yoldas, P.W. Partlow, Thin Solid Films 129 (1985) 1.
[33] W.D. Kingery, H.K. Bowen, D.R. Uhlmann, Introduction to Ceramics, Wiley, New York, 1976, p. 669.
[34] J.F. Nye, Physical Properties of Crystals: Their Representation by Tensors and Matrices, Oxford Science, New York, 1992.
[35] W. Lukosz, P. Pliska, Opt. Commun. 117 (1995) 1.
[36] H. Hunsche, M. Vergöhl, H. Neuhäuser, F. Klose, B. Szyszka, T. Matthée, Thin Solid Films 392 (2001) 184.
[37] T. Yamamoto, T. Shiosaki, A. Kawabata, J. Appl. Phys. 51 (6) (1980) 3113.
[38] J. Yu, X. Zhao, Q. Zhao, Thin Solid Films 379 (2000) 2.
[39] S.S. Lin, J.L. Huang, J. Mater. Res. 18 (2003) 1943.